Pergamon

Adv. Space Res. Vol. 19, No. 10, pp. 1577–1586, 1997

Printed in Great Britain
0273-1177/97 $17.00 + 0.00

PII: S0273-1177(97)00371-2

MODELING THE MOON'S EXTENDED SODIUM CLOUD AS A TOOL FOR INVESTIGATING SOURCES OF TRANSIENT ATMOSPHERES

Michäel Mendillo*, Joshua Emery*,** and Brian Flynn***

** Center for Space Physics, Boston University, 725 Commonwealth Avenue, Boston MA 02215, U.S.A.*
*** Currently at Department of Planetary Science, University of Arizona, Tucson AZ 85721, U.S.A.*
**** Center for EUV Astrophysics, University of California, Berkeley CA 94720, U.S.A.*

ABSTRACT

A review is presented of wide-angle, low-light-level imaging observations of the Moon's extended sodium atmosphere and Monte Carlo simulation studies used in their interpretation. The observational results at quarter and full Moon show dramatically different morphology patterns. The computer model results show that both morphologies are consistent with a single source function and subsequent dynamical evolution of the ejected sodium atoms. Different viewing geometries essentially account for the observational differences. We thus find no need to modify source rates significantly during full Moon periods when the terrestrial magnetosphere shields the lunar regolith from possible solar wind sputtering sources.

INTRODUCTION

Observational studies of the transient atmospheres of Mercury and the Moon have proceeded in parallel since their discovery a decade ago (Potter and Morgan, 1985,1988; Tyler et al., 1988). The modeling philosophy applied to both bodies has also been similar (Ip, 1986, 1990, 1991; Smyth, 1986; Smyth and Marconi, 1995a,b; Flynn and Mendillo, 1995), one of Monte Carlo simulations of multi-particle launch scenario trajectories. In each area, observations and models, the focus has been to determine how atmospheric morphology can be used to constrain and/or identify the source mechanisms responsible for the known atmospheric properties. While sodium (Na) and potassium (K) have been observed at both bodies, by far the most attention has been given to atmospheric processes illuminated by the presence of sodium.

The various sources and sinks for Na have been reviewed several times in the literature (Morgan and Shemansky, 1990; Sprague et al., 1992; Smyth and Marconi, 1995a,b, and references therein), and will be summarized only briefly here. Sodium atoms in a regolith can be sputtered from the surface by the impact of micrometeors, by ions in the solar wind, or by solar photons. Release can also occur by evaporation from the hot surface, or perhaps from chemical reactions (Potter, 1995). Once in motion above the surface, sodium atoms move in collision-free trajectories that can either lead to escape or return to the surface; pure capture orbits (ellipses or circles) are thought to be exceedingly rare. While aloft, Na can be ionized, effectively removing it from the atmosphere by solar wind entrapment and transport. Thus the phrase "transient atmosphere" is used to describe the situation of an atmosphere that is being continuously generated and continuously lost.

To some extent, all of the source processes noted above must occur on both the Moon and Mercury. The solar induced effects should scale with the inverse square of distance from the sun, while the micrometeor flux at 0.4 and 1.0 AU remains poorly understood. The role played by magnetic fields is also different at each body. At Mercury, the solar wind is probably shielded from reaching the surface by the presence of the planet's dipole field. It is a weak field, however, and thus various entry points may occur and change with time (Sprague, 1992; Ip, 1993). At the Moon, there is no appreciable intrinsic magnetic field to obstruct solar wind impact, but the Moon does spend approximately 4 days/month within the Earth's magnetosphere and therefore out of contact with direct solar wind particles (Potter and Morgan, 1994). Yet, magnetospheric energetic particle populations are present and variable during these episodic geomagnetic tail crossings.

In this paper, we will describe the lunar sodium atmosphere as a test case transient atmosphere. The Moon is a conveniently nearby laboratory-in-space for observational studies of sources that also act at Mercury. While differences other than scaling with distance from the Sun surely exist, the lunar case study, with intrinsic interest in its own right, should have a scientific yield related to Mercury, as well as to other primitive bodies.

WIDE-ANGLE IMAGING OF THE MOON'S EXTENDED ATMOSPHERE

To date, the large-scale morphology of the Moon's sodium atmosphere has been observed only by our group at Boston University (Mendillo et al, 1991, 1993; Flynn and Mendillo, 1993; Mendillo and Baumgardner, 1995). This is unfortunate in the sense that scientific investigations benefit by independent observations that verify and/or challenge similar data sets. The instrumentation required to conduct coronagraph-type observations of extended planetary atmospheres has been described in Baumgardner et al. (1993). For the lunar case, the technique has been limited to a few days near quarter Moon due to scattered light at gibbous and full Moon times, and to sky brightness and low elevation/long path lengths through the terrestrial atmosphere at crescent Moon (Mendillo et al., 1993). A notable exception occurs during a total lunar eclipse when the extended Na cloud at full Moon can be observed during the approximately 80 minutes of totality (Mendillo and Baumgardner, 1995).

Figure 1 illustrates the two patterns obtained during quarter and full Moon conditions. To describe the radial behavior of Na (D1+D2) brightness as a function of solar zenith angle, we have adopted the practice of using power law functions of the form

$$I(r, \chi) = I_o(\chi)\, r^{\alpha(\chi)} \tag{1}$$

where I is brightness in Rayleighs (R), r is distance measured in units of the lunar radius (R_m), α is the power law index, χ is the solar zenith angle, and I_o is effective or extrapolated brightness just above the limb of the Moon (i.e., at r = 1). For the quarter Moon case, Flynn and Mendillo (1993) found these parameters to be

$$I_o(\chi) = (1 + 6\,\mathrm{Cos}^2\,\chi) \text{ kilo-Rayleighs (kR)} \tag{2}$$

$$\alpha(\chi) = -2\,(1 + \cos^2\chi) \tag{3}$$

For the full Moon case, Mendillo and Baumgardner (1995) found $I_o \simeq 1$ kR and $\alpha \simeq -2$ at all χ values. Thus, at quarter Moon, when χ is essentially latitude, there is a strong gradient in both brightness and in

its radial dependence from $\chi = 0°$ (sub-solar limb above the equator) to χ=90° (limb above the poles). At full Moon, where $\chi = 90°$ at all points along the limb, there is an essentially radially symmetrical "extended atmosphere." In both cases, the term extended atmosphere refers to distances at least 0.5 R_m above the limb, that is, to the $r > 1.5$ R_m areas sampled by our coronagraph system. The population of Na atoms so sampled must be "hot" or "superthermal" to reach these substantial heights before loss by ballistic escape, return to the surface or by photoionization.

In summary, two sets of observations show that the derived parameters for effective limb brightness and its radial power law are the same at $\chi = 90°$, referring to the poles at quarter Moon and all positions at full Moon. We now turn to modeling studies to see if these morphologies are consistent with a single source function. That is, can the observations at quarter and full Moon be described by the same simulated atmosphere viewed under different Earth-Moon-Sun geometries?

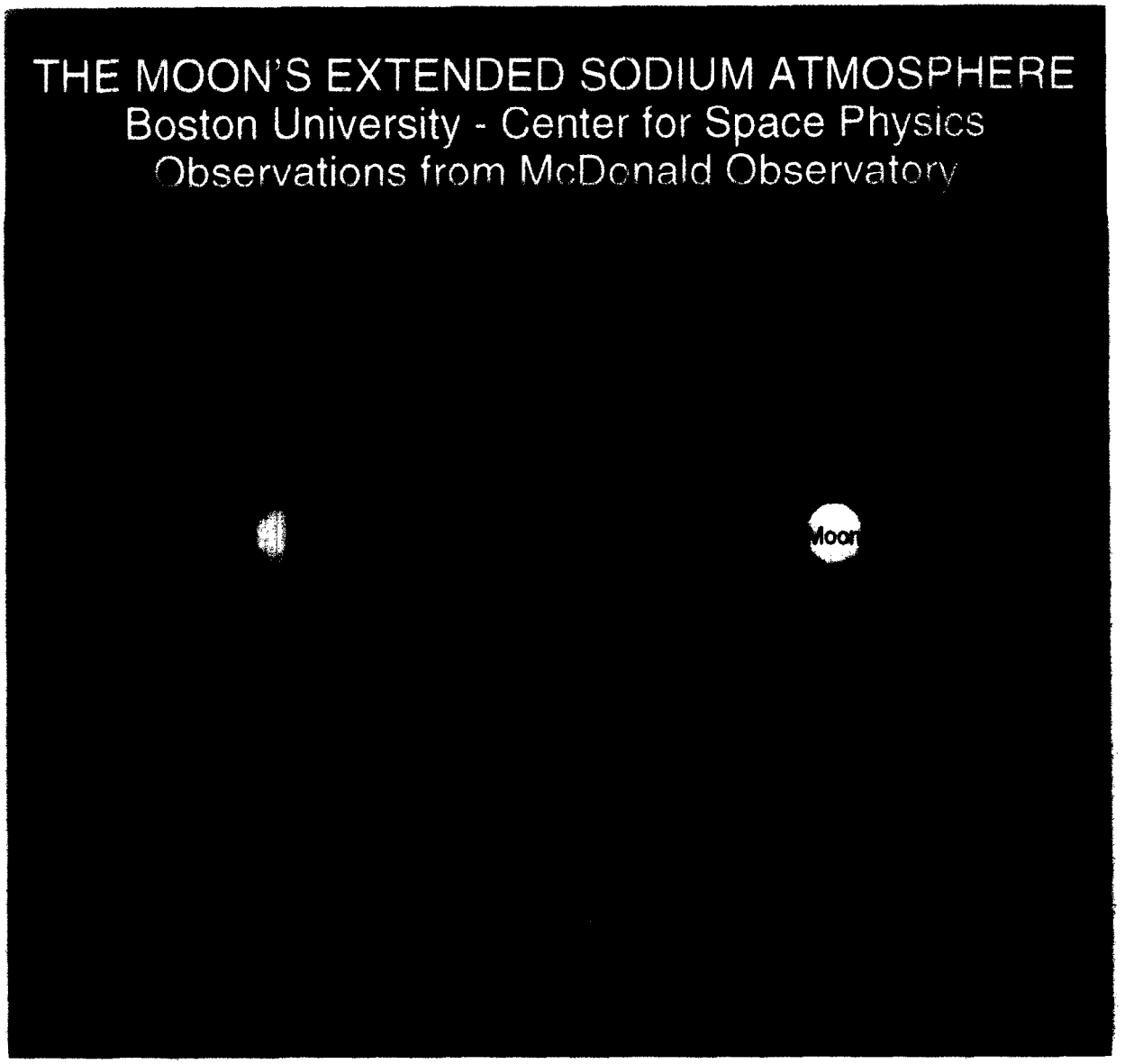

Fig. 1: The extended atmosphere of the Moon as portrayed in sodium (D1+D2) emission under conditions of quarter and full phase

SIMULATION STUDIES

Our Monte Carlo model of the Moon's sodium atmosphere has been described by Flynn and Mendillo (1995). Briefly, the model produces a steady state atmosphere from Maxwellian production functions for sodium ejected from the surface that can be either spatially uniform or with a solar zenith angle dependence on the dayside hemisphere. The loss processes included are direct escape, adsorption upon return to the surface and photoionization while aloft. In addition to gravity, solar radiation pressure also acts upon the atoms that are in sunlight. The application of this model to the quarter Moon conditions of 30 September 1991 shown in Figure 1 offered several insights to the Na source mechanism issue (Flynn and Mendillo, 1995):

(1) A spherically uniform source yields the least acceptable fit to the observed morphology pattern, as described by the parameters I_o and α of equation (1). While the uniform source, and indeed any other "reasonable" source, could be adjusted (by varying the temperature of the Maxwellian source function) to give the r^{-4} brightness decrease at the sub-solar point, it was at other zenith angles (latitudes) that the model diverged markedly from the data. This was interpreted as evidence that a source that might be spatially uniform (e.g., micrometeors) could not be the dominant mechanism that produces the Moon's extended Na coma.

(2) Hemispheric (dayside) source functions that decreased with increasing solar zenith angle were better able to match observations of a strong decrease in limb brightness (I_o) and radial power law index (α). Solar wind and photon sources are likely candidates for such types of sources. While the agreement between model and data was far from ideal, the $\cos^2 \chi$ source dependence did capture the essential patterns observed under quarter Moon conditions. However, we note that radiation pressure also contributes to angular (latitudinal) structure (Ip 1993; Smyth and Marconi 1995b) and so the latitudinal profiles of brightness do not relate uniquely to the latitudinal dependence of sources.

We now investigate if the same $\cos^2 \chi$ source can also account for the lunar Na atmosphere observed at the time of full Moon. To do this, we compare model runs appropriate to the 30 September 1991 and 29 November 1993 images in Figure 1. The only significant difference between the model inputs for these two dates is a small change in the Moon's velocity with respect to the Sun, an effect that results in a small change in solar radiation pressure acceleration upon the Na atoms (Smyth and Marconi, 1995b). The 3-dimensional nature of the Monte Carlo simulation code allows for the resultant sodium coma and tail to be viewed from any direction. Figure 2 shows the case of the 30 September 1991 viewed from the Earth as its actual quarter Moon pattern, as well as from an equivalent distance along the luni-solar axis to show its simultaneous full Moon pattern. Two possible source mechanisms are shown, uniform and $\cos^2 \chi$ dependent, with brightness levels normalized to the observed pattern at quarter Moon in Figure 1. The effects of a more extended coma for the $\cos^2 \chi$ source are clearly evident. Since this pattern better matched the parameterization quantities I_o and α (Flynn and Mendillo, 1995), we used the $\cos^2 \chi$ source to model the 29 November 1993 case as well.

The results for both quarter Moon simulations are given in Figure 3, and both full Moon simulations in Figure 4. The power law index (α) and equivalent limb brightness I_o parameters extracted from the simulated images are given in the bottom panels. The $\chi = 90°$ values for the limb above the poles at quarter Moon (Figure 3) and at all limb positions at full Moon (Figure 4) are noted below each figure. We draw the following conclusions from these analyses: (1) Given the discretized nature of Monte Carlo methods, we characterize the simulation results for both events as essentially identical. (2) At 90° zenith angles, the effective limb brightness from both runs was $I_o \simeq 1.8$ kR, with a power law index of $\alpha \simeq -2.5$.

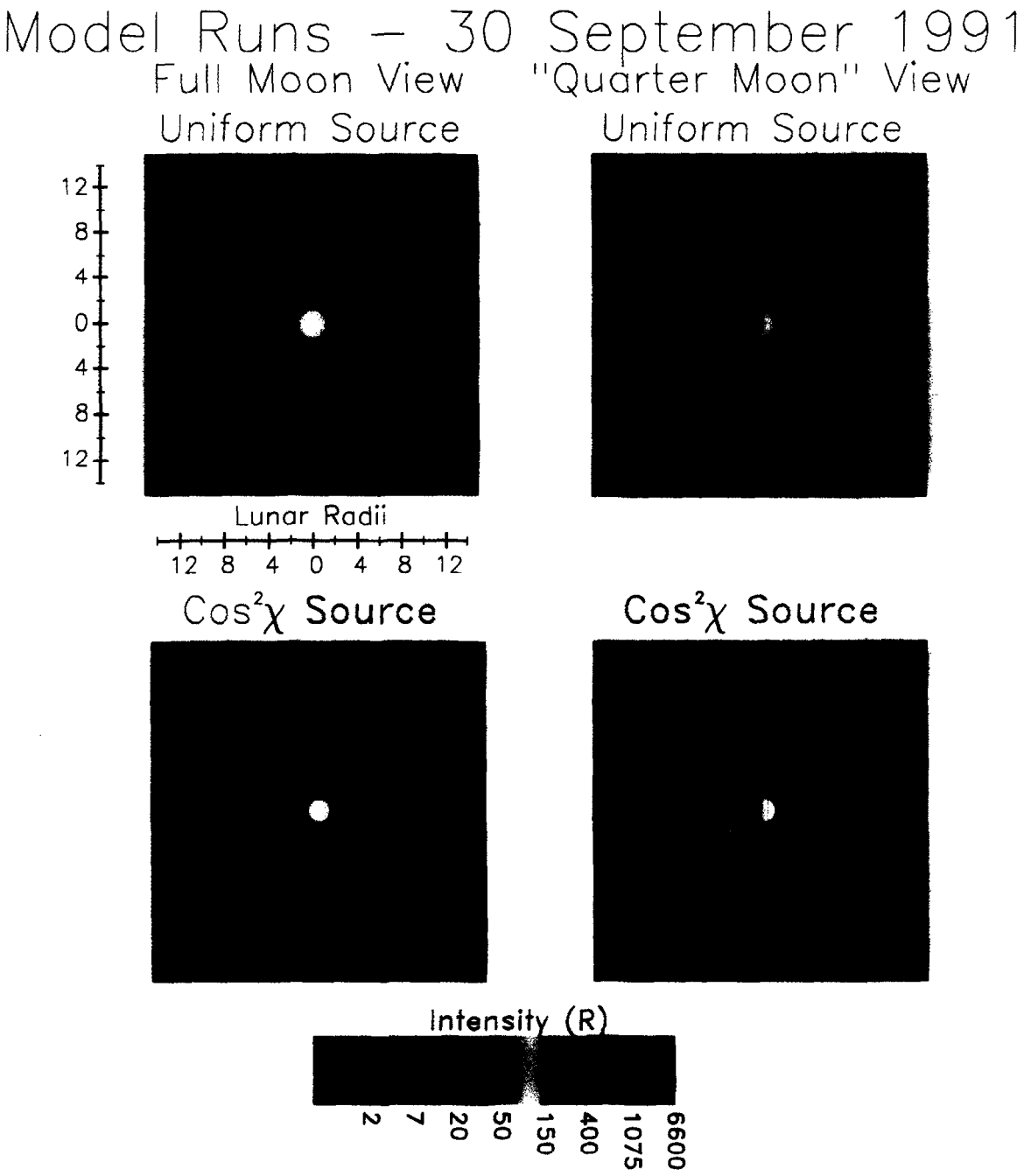

Fig. 2: Simulation of the Moon's extended sodium atmosphere for conditions of 30 September 1991. The results are given as equivalent images in Rayleighs (R) for full Moon (left) and quarter Moon (right) viewing conditions. The source functions used were spatially uniform (top) and hemispheric (dayside) with $\cos^2 \chi$ dependence on solar zenith angle (χ).

The observations in Figure 1, as summarized in the Introduction, have I_o = 1 kR and α = -2 at χ = 90°. Thus, we conclude from both investigations, simulation and observation, that the lunar atmosphere is essentially constant in gross structure. The difference in appearance at quarter and full phase is essentially due to different geometrical viewing conditions. Variability in the extended sodium atmosphere must occur at some time and altitude scales, but these are not apparent from our limited samples to date. In particular, the presence of an extended lunar atmosphere at full Moon phase that is comparable to its pattern at quarter phase suggests that magnetospheric shielding of solar wind impact is of minor consequences. Thus, solar wind sputtering cannot be the dominant source mechanism for releasing fast Na atoms from the lunar regolith, as suggested by Potter and Morgan (1994).

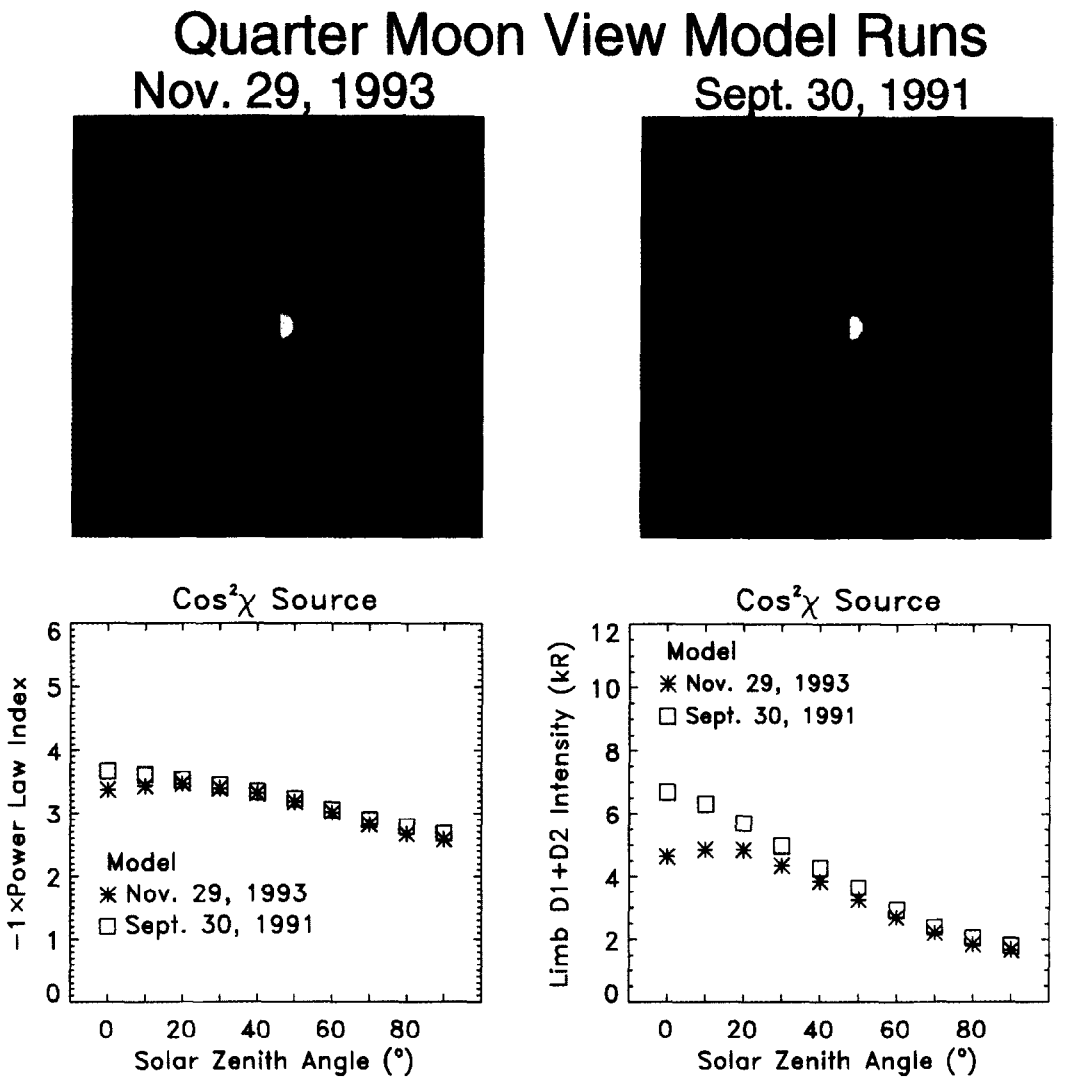

Fig. 3: Comparison of simulation results for the quarter Moon case of 30 September 1991 with the equivalent quarter Moon view obtained from the full Moon conditions of 29 November 1993. Note: Values at 90° zenith angle give power law index (α) = -2.7 and -2.6 and limb brightness (I_o) = 1.8 and 1.7 kR.

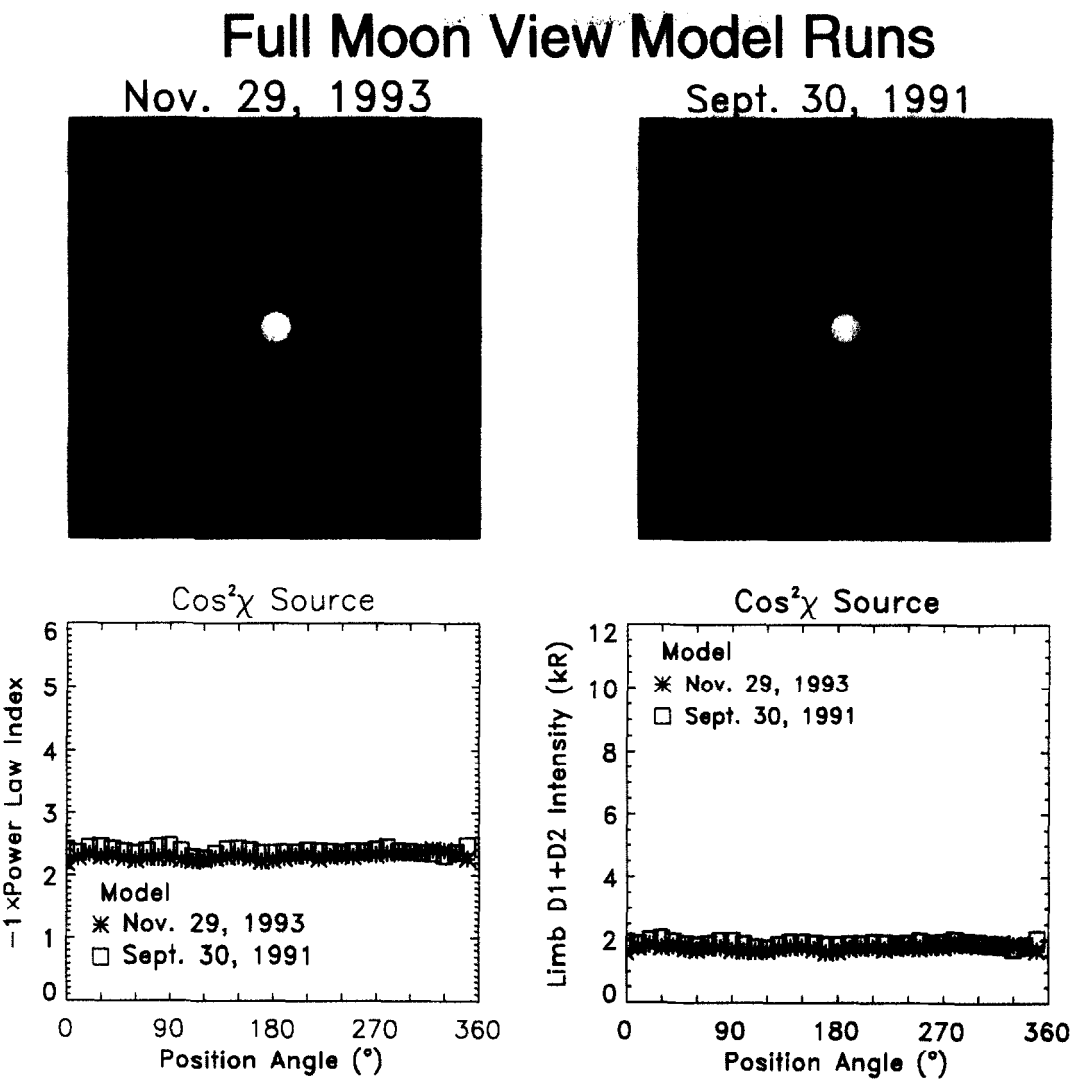

Fig. 4: Comparison of simulation results for the full Moon case of 29 November 1993 with the equivalent full Moon view obtained from the quarter Moon conditions of 30 September 1990. Note: Values at 90° zenith angle give power law index (α) = -2.4 and -2.3 and limb brightness (I_o) = 1.9 and 1.7 kR.

DISCUSSION

The simulation results summarized above were cast in terms of the morphology parameterization quantities I_o and α. While the simulation grid extended from 1 R_m (limb) to ± 15 R_m, the derivations of I_o and α were done over the distance range 1.5 to 4.0 R_m. This coincides with the domain of maximum reliability of the model (as discussed in Flynn and Mendillo, 1995), as well as with the best signal-to-noise regions of the observations (i.e., out to the 10-20 R brightness levels). Figure 5 presents simulation results for the full field of view (top) as well as from distances closer to the Moon, i.e., within the first lunar radius (1750 km) above the surface (bottom panel). Here the model results come from many test particle trajectories and thus the morphology pattern is very well described. There is an interesting change in radial behavior within the first half radius in height. Beyond 1.5 R_m, where our data occur, the radial pattern of brightness

is fairly linear on a log-log plot, showing that a well defined α value can be obtained. For example, the radial profile at quarter Moon (position A, solid line) is parallel to an analytical expression of index $\alpha = -4$ (dash-dot line). Similarly, the $\chi = 90°$ results at positions B and C are also fairly linear, resulting in $\alpha = -2.5$. However, the extrapolated limb brightness (I_o) levels using model results from 1.5 to 4 Rm fall below the actual computed values at the limb. This is due to the extrapolations coming from distant regions where only high speed ejected atoms can go. As shown in Figure 1 of Flynn and Mendillo (1995), reproduced in part here as Figure 6, only the high speed tail population of the 1400° K Maxwellian distribution produces the extended coma. The bulk of the particles stay at lower heights. This causes a noticeable departure from the quasi-linear profiles in Figure 5, particularly at the sub-solar point for quarter Moon conditions (position A, solid line). At heights of 300-500 km (1.2-1.3 R_m), the fall-off in brightness is steeper than the r^{-4} pattern; this is equivalent to a smaller scale height in an exponential atmosphere portrayal of data. Observational and theoretical evidence exists for such "double scale height" or "dual temperature" patterns (Kozlowski et al., 1990; Sprague et al., 1992; Stern and Flynn, 1995), and these are usually described in terms of hot and cold populations resulting from different mechanisms (e.g., thermal desorption and sputtering). While a single Maxwellian population is used in our model studies as a mathematically-convenient way to input a population of ejected atoms, it is of interest to see that their subsequent altitude separation produce brightness patterns that mimic two separate thermal populations.

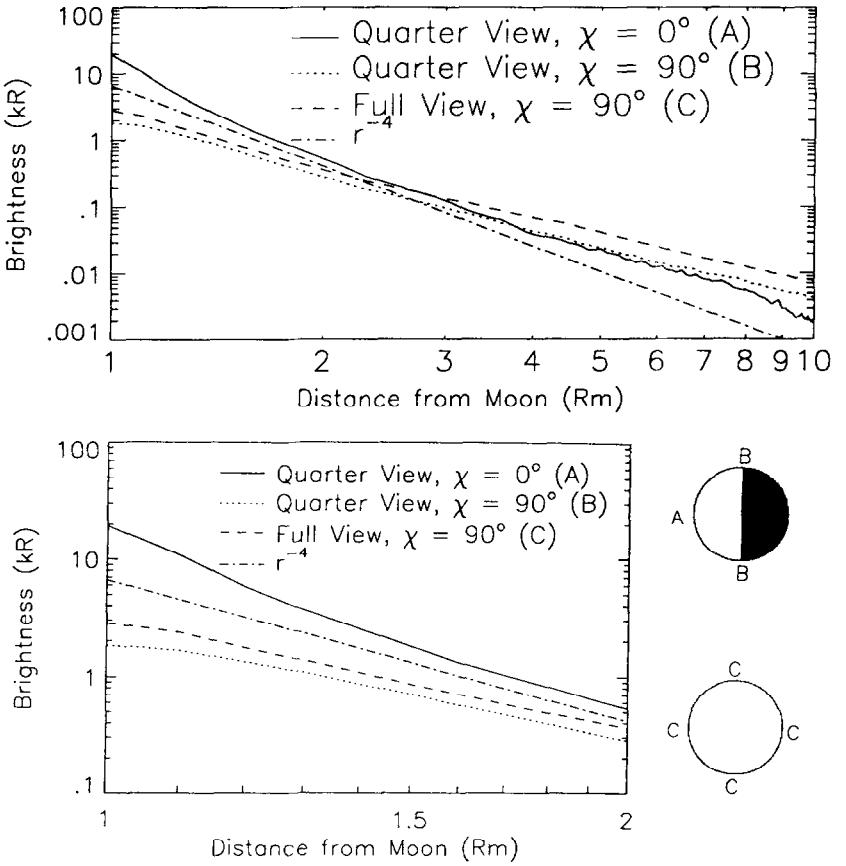

Fig. 5: (Top panel) Full simulation results for the case of 30 September 1991 parameterized in earlier figures. The model brightness levels are compared under different viewing conditions of quarter and full Moon phase over a scale of 10 lunar radii.
(Bottom panel). Expanded version of near-Moon results showing the departure from quasi-linear behavior at $r \leq 1.3\ R_m$. (See text.)

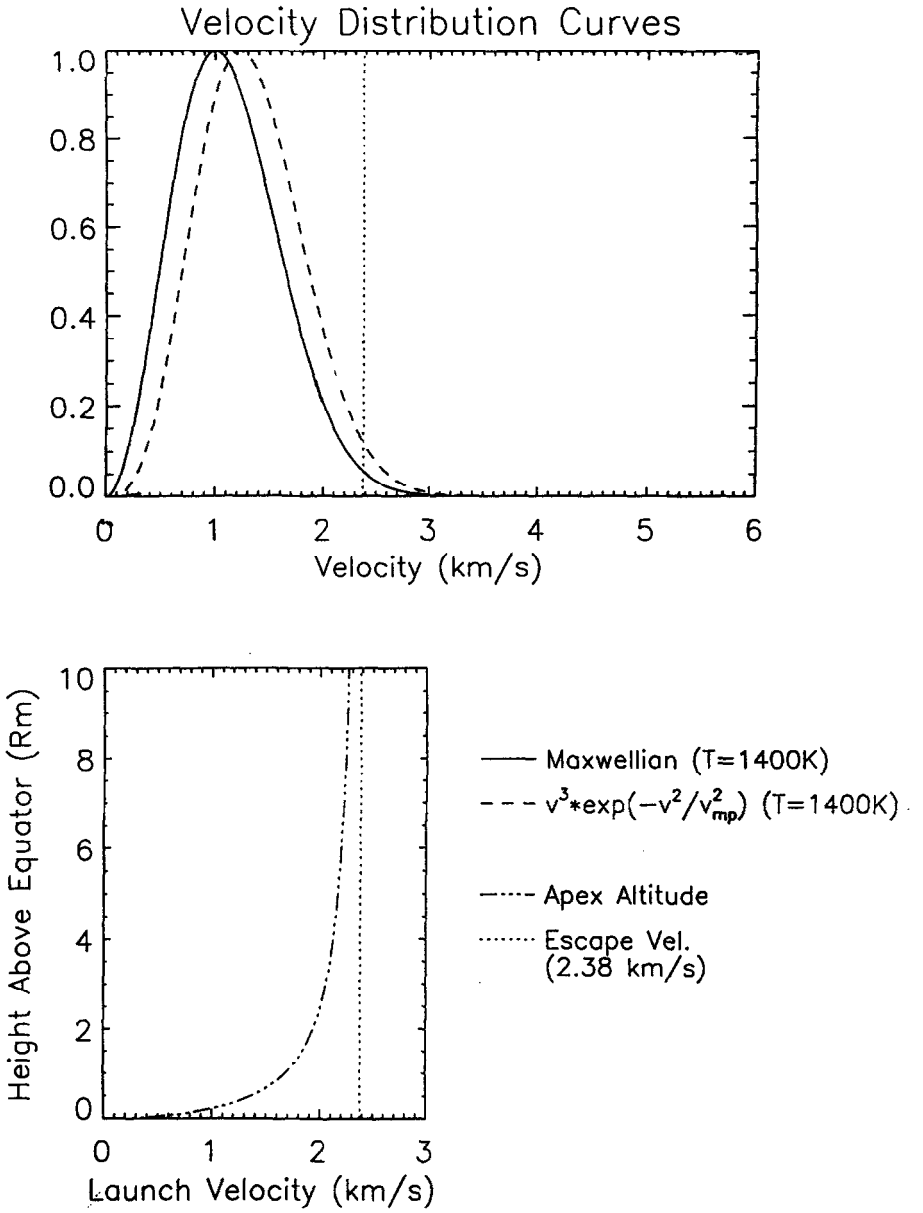

Fig. 6: Source characteristics for the model. (Top panel) Normalized Maxwellian and modified Maxwellian velocity distributions from which the pseudo-random launch velocities are chosen. Both curves have a most probable velocity corresponding to a temperature of 1400° K. (Bottom panel) Maximum height reached (apex altitude) for a sodium atom launched vertically from the lunar surface, neglecting radiation pressure effects. The lunar escape velocity is marked on both plots for references (after Flynn and Mendillo, 1995).

Acknowledgment. We are grateful for discussions with J. Baumgardner and acknowledge support for this work from NASA's Planetary Astronomy Program and from the Center for Space Physics at Boston University.

REFERENCES

Baumgardner, J., B. Flynn, and M. Mendillo, Optical Eng., 32,3028, (1993).
Flynn, B., and M. Mendillo, Science, 261, 184, 1993
Flynn, B., and M. Mendillo, J. Geophys. Res., 100, 23271, (1995).
Ip, W.-H., Geophys. Res. Lett., 13, 423, (1986).
Ip, W.-H., Ap. J., 356, 675, (1990).
Ip, W.-H., Geophys. Res. Lett., 18, 2093, (1991).
Ip, W.-H., Ap. J., 418, 451, (1993).
Kozlowski, R. W. H., A. L. Sprague, and D. M. Hunten, Geophys. Res. Lett., 2253, (1990).
Mendillo, M., J. Baumgardner, and B. Flynn, Geophys. Res. Lett., 18, 2097, (1991).
Mendillo, M., B. Flynn, and J. Baumgardner, Adv. Space Res. 13, 313, (1993).
Mendillo, M., and J. Baumgardner, Nature, 377, 404, (1995).
Morgan, T. H., and D. E. Shemansky, J. Geophys. Res., 96, 1351, (1991).
Potter, A. E., Geophys. Res. Lett., 22, 3289, (1995).
Potter, A. E., and T.H. Morgan, Science, 229, 651, (1985).
Potter, A. E., and T. H. Morgan, Geophys. Res. Lett., 15, 1515, (1988).
Potter, A. E., and T. H. Morgan, Geophys. Res. Lett., 21, 2263, (1994).
Smyth, W.-H., Nature, 323, 696, (986).
Smyth, W.-H., and M. L. Marconi, Ap. J., 441, 839, (1995a).
Smyth, W.-H. and M. L. Marconi, Ap. J., 371, (1995b).
Stern, S. A., and B. C. Flynn, Ast. J., 109, 835, (1995)
Sprague, A., Icarus, 84, 93, 1990, J. Geophys. Res. Planets, 97 (E11), 18257, (1992).
Sprague, A., R Kozlowski, D. Hunten, W. Wells, and R. Grosse, Icarus, 96, 27, (1992).
Tyler, A., R. Kozlowski, and D. H. Hunten, Geophys. Res. Lett., 15, 1141, (1988).